The Journal of Chemical Physics

Resolution-of-the-identity second-order Møller–Plesset perturbation theory with complex basis functions: Benchmark calculations and applications to strong-field ionization of polyacenes

Cite as: J. Chem. Phys. **152**, 174103 (2020); https://doi.org/10.1063/5.0004843
Submitted: 17 February 2020 . Accepted: 12 April 2020 . Published Online: 04 May 2020

Mario Hernández Vera, and Thomas-C. Jagau

View Online Export Citation CrossMark

Lock-in Amplifiers up to 600 MHz Watch

© 2020 Author(s).

The Journal of Chemical Physics ARTICLE scitation.org/journal/jcp

Resolution-of-the-identity second-order Møller–Plesset perturbation theory with complex basis functions: Benchmark calculations and applications to strong-field ionization of polyacenes

Cite as: J. Chem. Phys. 152, 174103 (2020); doi: 10.1063/5.0004843
Submitted: 17 February 2020 • Accepted: 12 April 2020 •
Published Online: 4 May 2020

View Online Export Citation CrossMark

Mario Hernández Vera and Thomas-C. Jagau[a)]

AFFILIATIONS

Department of Chemistry, University of Munich (LMU), D-81377 Munich, Germany

[a)]Author to whom correspondence should be addressed: th.jagau@lmu.de

ABSTRACT

We study the performance of the resolution-of-the-identity (RI) approximation for complex basis functions that we recently introduced [M. Hernández Vera and T.-C. Jagau, J. Chem. Phys. **151**, 111101 (2019)] for second-order Møller–Plesset (MP2) perturbation theory as well as for the Coulomb and exchange contributions in Hartree–Fock theory. The sensitivity of this new RI-MP2 method toward the basis set and the auxiliary basis set is investigated, and computation times are analyzed. We show that the auxiliary basis set can be chosen purely real, that is, no complex-scaled functions need to be included. This approximation enables a further speedup of the method without compromising accuracy. We illustrate the application range of our implementation by computing static-field ionization rates of several polyacenes up to pentacene ($C_{22}H_{18}$) at the RI-MP2 level of theory. Pronounced anisotropies are observed for the ionization rates of these molecules.

Published under license by AIP Publishing. https://doi.org/10.1063/5.0004843

I. INTRODUCTION

Electronic resonances[1,2] play a fundamental role in molecular strong-field phenomena, such as high-harmonic generation,[3–5] above-threshold ionization,[6,7] and laser-induced electron diffraction.[8–10] These phenomena are driven by ionization processes whose modeling is computationally demanding, and as a result, accurate and reliable theoretical data remain elusive for many molecules. Often, ionization processes are studied with time-dependent (TD) approaches. Since the numerical integration of the full three-dimensional electronic Schrödinger equation is only possible for systems with very few electrons,[11–13] approximations need to be employed. For example, the TD configuration interaction singles (TD-CIS) approximation, in which the wave function is restricted to a linear combination of singly excited Slater determinants, has been successfully used to characterize the electronic dynamics in polyatomic molecules exposed to laser pulses of different strengths and polarization.[14–17] TD density functional theory (TD-DFT) has been used for the same purpose as well.[18–21]

Time-dependent approaches provide a full picture of the ionization dynamics, but the propagation of the wave function over sufficiently long times demands large computational resources. In addition, since the number of particles is conserved for a Hermitian Hamiltonian, special techniques from non-Hermitian quantum mechanics[1] need to be employed to model the actual loss of electrons and not just spatial separation from the system. Noteworthy is especially the use of complex absorbing potentials (CAPs)[22–25] and complex-scaling techniques.[26–31]

The high computational cost of TD methods motivates the development of time-independent approaches for molecular strong-field ionization. In the tunnel ionization regime, that is, for low frequencies and high intensities of the electromagnetic field, ionization can be treated as if it took place in a static field.[1,32] Under

Published under license by AIP Publishing

these conditions, the ionization process can in many cases be described in terms of a single or a few Stark resonances.[1] Several analytical formulas have been proposed to compute molecular static-field ionization rates.[33–35] One state-of-the-art approach is, for example, weak-field asymptotic theory.[36–39] Further recent contributions use the hybrid antisymmetrized coupled-channels (haCC) approach[40,41] or combine single-electron approaches with the description of the molecular core in terms of an effective potential.[42,43]

An alternative powerful approach to compute static-field ionization rates consists in using electronic-structure methods originally devised for bound states.[2] This relies on the application of complex-scaling techniques to Stark resonances.[44–48] Molecules exposed to static electric fields do not hold bound states, but by scaling asymptotically the electronic coordinates in the molecular Hamiltonian as $\mathbf{r} \to \mathbf{r}e^{i\theta}$, the new eigenfunctions become L^2 integrable. A previously hidden Stark resonance can be described in terms of the new complex eigenvalue

$$E_{\mathrm{res}} = E - i\,\Gamma/2, \tag{1}$$

where E and Γ are the energy and ionization rate of the Stark resonance, respectively. This technique, known as exterior complex scaling (ECS),[49] holds several advantages: It is firmly established by a rigorous mathematical formalism, and it is applicable to molecules within the Born–Oppenheimer approximation in contrast to the original theory of complex scaling.[1]

For an implementation relying on a Gaussian basis set, it is convenient to use complex basis functions (CBFs) that mimic the ECS approach by complex scaling the basis functions.[50,51] In CBF methods, diffuse Gaussian functions of the form

$$\chi_\mu(\theta) = N_\mu\, S_\mu(r_A)\exp\left[-\alpha_\mu\, e^{-2i\theta}\, r_A^2\right] \tag{2}$$

are included among the basis functions. In Eq. (2), N_μ is a normalization constant, A is an atomic center, $r_A = r - A$, and S_μ is a real polynomial in the components of r_A that depends on the angular quantum numbers of χ_μ. The exponent α_μ is complex-scaled with θ as the scaling angle. CBFs have been implemented at the static-exchange,[52] Hartree–Fock (HF),[53–55] multiconfigurational self-consistent field,[56] configuration interaction,[57,58] second-order Møller–Plesset (MP2),[59] and coupled-cluster singles and doubles (CCSD) levels of theory.[59] These methods have been used to study autoionizing[52,55,59] and Stark resonances.[60]

We recently took steps to extend the application range of CBFs to larger molecules. We introduced a generalized Schwarz inequality to screen two-electron integrals over complex-scaled basis functions,[61] and we also devised a resolution-of-the-identity (RI) MP2 method.[62] For the latter purpose, we employed an RI approximation[63–69] for the two-electron four-center electron-repulsion integrals (ERIs) over CBFs that appear in the expression for the MP2 correlation energy and in the Coulomb and exchange contributions in HF theory. This method yielded ionization rates that were in good agreement with rates from canonical MP2 theory and CCSD. At the same time, the reduction in computation time allowed us to describe Stark resonances of larger molecules such as benzene and naphthalene.

Yet, a more detailed analysis of this new RI-MP2 method is required to assess its performance, accuracy, and application range. This is the purpose of the present article. The remainder is organized as follows: Sec. II provides a brief description of the method; in particular, we show that a purely real auxiliary basis set is appropriate to approximate the ERIs over CBFs. In Sec. III, we assess the accuracy of the method with respect to the choice of the basis set and auxiliary basis set and analyze computation times of ionization rates for molecules of different sizes. In Sec. IV, we apply our RI-MP2 method to compute static-field ionization rates for several polyacene molecules to illustrate its application range. Section V presents our general conclusions.

II. RI-MP2 WITH COMPLEX BASIS FUNCTIONS

We presented the theory and our implementation of the RI-MP2 method with CBFs in our previous publication.[62] The theory relies on a complex-valued generalization of the functional by Dunlap[65] that reduces to the standard formulation from Hermitian quantum chemistry when the scaling angle θ is zero. Our implementation builds on the general implementation of CBFs by White, Head-Gordon, and McCurdy in the Q-Chem program package[70] reported in Ref. 52. The RI-MP2 and RI-HF working equations are formally the same as in the Hermitian theories except that a Takagi factorization is employed for the integrals $J_{PQ} = \int dr_1 \int dr_2\ \chi_P(r_1)\,\chi_Q(r_2)\,r_{12}^{-1}$ over the auxiliary functions χ_P and χ_Q, some of which are complex scaled.

The θ-dependence introduced by the finite basis set is corrected approximately according to[71]

$$E'_{\mathrm{res}}(F,\theta) = E_{\mathrm{res}}(F,\theta) - E_{\mathrm{res}}(F=0,\theta) + E_{\mathrm{res}}(F=0,\theta=0), \tag{3}$$

where F is the strength of the external static electric field. The optimal scaling angle θ_{opt} is determined from minimizing $|dE'_{\mathrm{res}}/d\theta|$.[1] In this work, we computed $E'_{\mathrm{res}}(F,\theta)$ at 14 different values of θ from 8° to 21° in steps of 1°. To find θ_{opt}, we performed a cubic spline interpolation between these values of $E'_{\mathrm{res}}(F,\theta)$. This procedure was repeated for all molecules and field configurations.

A. Use of real auxiliary basis functions (ABFs)

In the first applications of the RI-MP2 method, we used auxiliary basis sets that included diffuse complex-scaled Gaussian functions of the form of Eq. (2) and were about twice as large as the original basis sets.[62] Calculations with such auxiliary bases yielded ionization rates that generally agreed with canonical MP2 within 1%–2% and deviated by about 10% from CCSD. Computation times were reduced already considerably, in particular for RI-HF as compared to canonical HF.

In order to further increase the efficiency of the method, one can simply eliminate all complex-scaled auxiliary functions and use purely real auxiliary basis sets developed for standard Hermitian RI-MP2 theory.[72] This makes only a negligible impact on the accuracy of the results. To clarify why this is possible, we take a closer look at the RI approximation for CBF methods. The product of two Gaussian basis functions is expanded as

$$\chi_\mu\,\chi_\nu \approx \sum_P^{N_{\mathrm{fit}}}\left[\mathrm{Re}(d_P^{\mu\nu}) + i\,\mathrm{Im}(d_P^{\mu\nu})\right]\chi_P(\mathbf{r}),$$
$$\chi_\mu\,\chi_\nu \in \mathbb{C},\ d_P^{\mu\nu} \in \mathbb{C},\ \chi_P \in \mathbb{R}. \tag{4}$$

Published under license by AIP Publishing

Since the expansion coefficients $d_P^{\mu\nu}$ are complex, the real and imaginary parts of the product $\chi_\mu\chi_\nu$ can be represented in an auxiliary basis set $\{\chi_P\}$ that is purely real.

The expansion coefficients are then given in analogy to the Hermitian RI approximation as[73]

$$\begin{aligned}\mathrm{Re}(d_Q^{\mu\nu}) &= \sum_P (\mathrm{Re}(\mu\nu)|P)\left[\mathbf{J}^{-1}\right]_{PQ},\\ \mathrm{Im}(d_Q^{\mu\nu}) &= \sum_P (\mathrm{Im}(\mu\nu)|P)\left[\mathbf{J}^{-1}\right]_{PQ},\end{aligned} \tag{5}$$

where the integrals $J_{PQ} = \int dr_1 \int dr_2\ \chi_P(r_1)\,\chi_Q(r_2)\,r_{12}^{-1}$ are now real. Using Eqs. (4) and (5), we arrive at the RI approximation for the two-electron four-index ERIs defined using the c-product of non-Hermitian quantum mechanics.[74] The ERIs can be split into real and imaginary parts as

$$\begin{aligned}&\mathrm{Re}(\mu\nu|\sigma\lambda) + i\,\mathrm{Im}(\mu\nu|\sigma\lambda)\\ &\quad\approx (\mathrm{Re}(\mu\nu)|\mathcal{P}|\mathrm{Re}(\sigma\lambda)) - (\mathrm{Im}(\mu\nu)|\mathcal{P}|\mathrm{Im}(\sigma\lambda))\\ &\qquad + i(\mathrm{Im}(\mu\nu)|\mathcal{P}|\mathrm{Re}(\sigma\lambda)) + i(\mathrm{Re}(\mu\nu)|\mathcal{P}|\mathrm{Im}(\sigma\lambda)),\end{aligned} \tag{6}$$

where $\mathcal{P}$ is a projection onto the space spanned by the real auxiliary functions,

$$\mathcal{P} = \sum_{PQ} |\chi_P\rangle \left[\mathbf{J}^{-1}\right]_{PQ} \langle\chi_Q|. \tag{7}$$

Equation (6) shows that, using a real auxiliary basis set, the RI approximation for ERIs over CBFs can be decomposed into four real-valued RI approximations for the real and imaginary components of the Gaussian product. We point out, however, that this separation is not carried out explicitly in our implementation, where we work with complex arithmetic taking advantage of the Gaussian product rule. A further analysis of the functional form of the product of two CBFs is presented as Appendix to this article.

III. BENCHMARK CALCULATIONS

A. Real vs complex-scaled auxiliary basis functions

To illustrate numerically the validity of using only real-valued auxiliary basis functions, we present in Table I ionization rates for CO and C_6H_6 (benzene). We computed RI-MP2 ionization rates for these two molecules at a static field strength of $F = 0.06$ a.u. and different orientations of the field. Table I shows that the differences between ionization rates computed with auxiliary basis sets that are purely real or partially complex scaled typically stay below 1% for both molecules. This confirms that standard auxiliary basis sets without complex-scaled functions can be used in CBF-RI-MP2 calculations without losing accuracy. It is worth noting that in these calculations the auxiliary basis set roughly comprises the same number of functions as the original basis set, which is in contrast to recommendations for standard RI-MP2 calculations.[68,72,75]

To further corroborate the accuracy of the method, we compare in Fig. 1 RI-MP2 ionization rates for CO and N_2 with those obtained at higher levels of theory. As observed previously,[62] RI-MP2 reproduces canonical MP2 very well within 1%–2% and there is also good agreement with CCSD with the deviation typically staying below 10%.

We also included HF and RI-HF rates in Fig. 1 to illustrate the impact of electron correlation on the ionization rates. Most obviously, the anisotropy of Γ is not captured by a HF description, in particular at the lower field strengths. For N_2 at $F = 0.065$ a.u. and $\phi = 0^\circ$ (the field oriented along the molecular axis), the correlated

TABLE I. Ionization rates of CO and C_6H_6 (benzene) in atomic units at $F = 0.06$ a.u. computed with RI-MP2 using real and partially complex-scaled auxiliary basis functions (ABFs). Δ is the percentage difference between the rates.

	CO			C_6H_6		
ϕ (deg)[a]	Complex ABFs[b]	Real ABFs[b]	Δ	Complex ABFs[c]	Real ABFs[c]	Δ
0	0.000 794	0.000 787	0.9	0.014 582	0.014 582	0.0
15	0.000 747	0.000 740	0.9	0.015 280	0.015 279	0.0
30	0.000 660	0.000 654	0.9	0.016 469	0.016 460	0.1
45	0.000 589	0.000 584	0.9	0.017 912	0.017 904	0.0
60	0.000 494	0.000 489	1.0	0.018 293	0.018 216	0.4
75	0.000 368	0.000 365	0.8	0.017 200	0.017 182	0.1
90	0.000 271	0.000 268	1.1	0.016 691	0.016 675	0.1
105	0.000 202	0.000 193	4.7			
120	0.000 175	0.000 174	0.6			
135	0.000 195	0.000 196	0.5			
150	0.000 258	0.000 252	2.3			
165	0.000 326	0.000 325	0.3			
180	0.000 364	0.000 362	0.6			

[a] ϕ characterizes the orientation of the field; for CO, $\phi = 0^\circ$ corresponds to the field pointing from C to O, and for C_6H_6, $\phi = 90^\circ$ corresponds to the field being perpendicular to the molecular plane and $\phi = 0^\circ$ corresponds to the field being in the molecular plane oriented along a σ_v plane.
[b] Computed with a basis set derived from aug-cc-pVQZ. See the supplementary material for details.
[c] Computed with a basis set derived from aug-cc-pVTZ. See the supplementary material for details.

Published under license by AIP Publishing

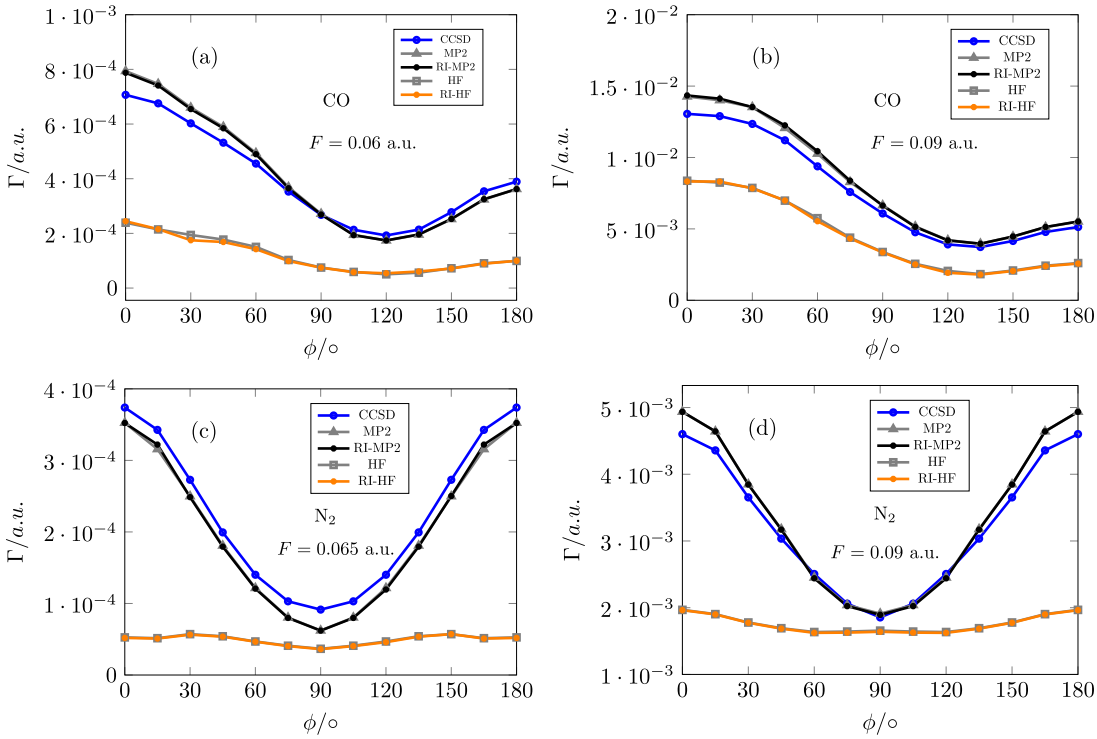

FIG. 1. Angle dependent ionization rates Γ of CO [panels (a) and (b)] and N_2 [panels (c) and (d)] at different field strengths computed at different levels of theory using a modified aug-cc-pVQZ basis set. RI-MP2 and RI-HF calculations were carried out using the standard RI-MP2-aug-cc-pVQZ auxiliary basis set. The orientation of the field with respect to the molecule is given by ϕ with $\phi = 0°$ corresponding to the field being parallel to the molecular axis. In panels (a) and (b), the field points from C to O at $\phi = 0°$. CCSD results are taken from Ref. 60.

methods deliver ionization rates that are up to seven times higher than those obtained with HF or RI-HF. At $\phi = 90°$ (the field perpendicular to the molecule), the deviation is much lower so that the anisotropy of Γ is not reproduced. At the higher field strength ($F = 0.09$ a.u.), the differences are somewhat smaller but still amount to a factor of 2.5 at $\phi = 0°$.

One may speculate that the angular dependence of the agreement between HF and correlated methods is related to a change in the contributions from different ionization channels to the overall Γ. It has been argued that ionization from σ orbitals is dominant at $\phi = 0°$, while contributions from π orbitals are more substantial at $\phi = 90°$.[16] This would mean that electron correlation makes a larger impact on the σ ionization channels than on those with π-symmetry, which is a plausible conclusion. A reliable analysis of this effect would, however, require the computation of partial ionization rates,[76] which is beyond the scope of the present work.

B. Truncation of the auxiliary basis set

It is also worthwhile to investigate how the agreement between RI-MP2 and MP2 deteriorates upon truncation of the auxiliary basis. The use of a smaller auxiliary basis set affords a reduction of computation times, but a compromise between accuracy and efficiency needs to be found. To analyze this aspect, we computed RI-MP2 ionization rates of CO and N_2 with three different auxiliary basis sets and compared them to canonical MP2 in Table II.

We can see that the differences between MP2 and RI-MP2 remain lower than 2% for both molecules when the standard RI-MP2-aug-cc-pVQZ auxiliary basis set is used. This good agreement reduces progressively when the auxiliary basis set is truncated. For both molecules, the eight shells of Gaussians with the highest angular momentum (two *f*-shells, four *g*-shells, and two *h*-shells) can be removed without affecting the accuracy considerably. Consistent with the higher absolute values of Γ for CO as compared to N_2, the agreement is better for CO, but the deviation stays below 10% for N_2 as well, and the anisotropy of Γ is captured correctly for both molecules. However, a further removal of eight diffuse shells (three *p*, three *d*, and two *f*) from the original auxiliary basis makes a strong impact on the results. While the anisotropy of Γ is still reproduced qualitatively and the results agree with canonical MP2 within a few percent at some orientations, there are also other orientations where the deviation is higher than 35%, rendering the results unreliable.

C. Cardinality of the basis set

In order to extend the application range of our RI-MP2 method to larger systems, it is important to establish how sensitive the ionization rates are toward the cardinality of the basis set and the

Published under license by AIP Publishing

TABLE II. Ionization rates of CO and N_2 in atomic units computed at field strengths of $F = 0.06$ a.u. and $F = 0.065$ a.u., respectively, using canonical MP2 and RI-MP2 with different auxiliary basis sets.

	CO				N_2			
ϕ (deg)[a]	Γ (MP2)	Γ(RI-MP2)[b]	Γ(RI-MP2)[c]	Γ(RI-MP2)[d]	Γ(MP2)	Γ(RI-MP2)[b]	Γ(RI-MP2)[c]	Γ(RI-MP2)[d]
0	0.000 793	0.000 787	0.000 764	0.000 762	0.000 352	0.000 352	0.000 332	0.000 474
15	0.000 746	0.000 740	0.000 718	0.000 721	0.000 315	0.000 322	0.000 301	0.000 433
30	0.000 660	0.000 654	0.000 633	0.000 649	0.000 249	0.000 248	0.000 236	0.000 336
45	0.000 589	0.000 584	0.000 566	0.000 593	0.000 180	0.000 179	0.000 168	0.000 240
60	0.000 494	0.000 489	0.000 474	0.000 508	0.000 121	0.000 120	0.000 110	0.000 162
75	0.000 369	0.000 365	0.000 353	0.000 390	0.000 080	0.000 079	0.000 070	0.000 108
90	0.000 271	0.000 268	0.000 261	0.000 301	0.000 062	0.000 062	0.000 052	0.000 084
105	0.000 248	0.000 193	0.000 236	0.000 272				
120	0.000 173	0.000 174	0.000 171	0.000 267				
135	0.000 195	0.000 196	0.000 196	0.000 298				
150	0.000 252	0.000 252	0.000 251	0.000 325				
165	0.000 323	0.000 325	0.000 322	0.000 408				
180	0.000 362	0.000 362	0.000 361	0.000 452				

[a] ϕ characterizes the orientation of the field with $\phi = 0°$ corresponding to the field being parallel to the molecular axis. For CO, the field points from C to O at $\phi = 0°$.
[b] Computed with the aug-cc-pVQZ+3s3p3d3f/cc-pVQZ basis set and RI-MP2-aug-cc-pVQZ auxiliary basis set.
[c] The same as *b* but with the most diffuse 2 *f*, 4 *g*, and 2 *h* shells removed from the auxiliary basis set.
[d] The same as *b* but with the most diffuse 3 *p*, 3 *d*, 4 *f*, 4 *g*, and 2 *h* shells removed from the auxiliary basis set.

number of diffuse functions included. This has been investigated previously at the CCSD and HF levels of theory for atoms and small molecules.[60,71] It was found that a further augmentation of the aug-cc-pVXZ basis sets by additional diffuse functions is indispensable to obtain accurate static-field ionization rates. In addition, lower ionization rates always require higher cardinality of the basis set.

The latter aspect is re-examined here. Table III shows RI-MP2 ionization rates for CO and N_2 computed with modified aug-cc-pVTZ and aug-cc-pVQZ basis sets. At the range of field strengths considered here ($F = 0.070$ a.u., 0.075 a.u., and 0.080 a.u.), Γ changes rapidly and depends strongly on the orientation. Moreover, since the lowest ionization potentials (IPs) of CO (14.23 eV and 17.16 eV) and N_2 (15.58 eV and 16.98 eV) are also quite different, the application of the same field strength entails a larger ionization rate for CO.

The results in Table III confirm that a basis set of triple-ζ quality is sufficient for a qualitatively correct description of ionization rates of the order of 10^{-3} a.u. or larger. For such cases, the deviations from the quadruple-ζ results usually amount to only a few percent and the anisotropy is captured correctly. However, for lower values of Γ, the triple-ζ basis becomes unreliable very quickly as the results for N_2 at the lower field strengths illustrate. This trend can be related to the fact that modeling a tunnel ionization process requires a correct description of the region through which the electron tunnels. As this region shrinks with increasing field strength when the molecular potential is distorted more and more, a less extended basis set with fewer functions becomes sufficient.

We note that the lowest ionization rates for N_2 reported in Table III are possibly not yet fully converged. For the H and He atoms, it was found previously[71] that quadruple-ζ and quintuple-ζ results differ by up to 8% for Γ values of 5×10^{-5} a.u., whereas for 5×10^{-4} a.u., they already agree within 1%–2%. Since the basis set dependence of Γ is related mainly to its order of magnitude and not to other specifics of the electronic structure, these findings also apply to N_2 and CO and can serve as an additional estimate for the accuracy of the values reported in Table III.

D. Computation times

The RI approximation for CBFs enables a significant speedup of the calculation of ionization rates at the HF and MP2 levels of theory even though the formal scaling of the operation count with respect to system size is not reduced. The speedup is substantial, in particular for RI-HF as compared to canonical HF. The reason is that CBF calculations always require large basis sets with many diffuse functions; the redundancy inherent to such bases is removed in an efficient manner through RI decomposition.[68,72,77]

To illustrate this property, we present in Fig. 2 representative computation times for the evaluation of a single complex energy for CO and $C_{14}H_{10}$ (anthracene). These data are not meant as a comprehensive and rigorous assessment of the performance of our implementation, which is not optimized in many regards; rather, we want to convey how much time is required to perform the computations reported in this article and, correspondingly, what the practical application range of our CBF-RI-MP2 method is.

Calculations for CO were done with a modified aug-cc-pVQZ basis set comprising 256 functions and two different auxiliary basis sets with 336 and 550 functions, respectively. Calculations for $C_{14}H_{10}$ were done with a modified aug-cc-pVTZ basis set comprising 1816 functions and two different auxiliary basis sets with 1944 and 3684 functions, respectively. For both molecules, the larger auxiliary basis sets contain several shells with complex-scaled exponents, while the smaller auxiliary basis sets are purely

Published under license by AIP Publishing

TABLE III. Ionization rates of CO and N_2 in atomic units computed with RI-MP2 and basis sets of aug-cc-pVTZ and aug-cc-pVQZ quality. Δ is the percentage difference between ionization rates computed with the two basis sets.

		CO			N_2		
F (a.u.)	ϕ (deg)[a]	Γ (RI-MP2)[b]	Γ (RI-MP2)[c]	Δ	Γ (RI-MP2)[b]	Γ (RI-MP2)[c]	Δ
0.070	0	0.002 818 8	0.003 139 4	10.2	0.000 263 0	0.000 721 7	63.5
	15	0.002 777 6	0.003 021 6	8.1	0.003 068 5	0.000 668 4	459.0
	30	0.002 565 2	0.002 702 6	5.1	0.000 702 4	0.000 520 2	35.0
	45	0.002 321 1	0.002 270 5	2.2	0.000 524 7	0.000 368 2	42.5
	60	0.002 013 3	0.001 883 0	6.9	0.000 403 6	0.000 258 5	56.1
	75	0.001 601 6	0.001 475 1	8.6	0.000 207 8	0.000 184 7	12.5
	90	0.001 186 5	0.001 125 4	5.4	0.000 131 2	0.000 152 0	17.7
0.075	0	0.004 846 8	0.005 170 1	6.2	0.001 185 0	0.001 301 1	8.9
	15	0.004 707 3	0.005 031 7	6.4	0.002 010 9	0.001 211 6	66.0
	30	0.004 377 5	0.004 814 7	9.1	0.001 078 1	0.000 973 3	10.8
	45	0.003 937 9	0.004 137 3	4.8	0.000 857 2	0.000 708 4	21.0
	60	0.003 298 2	0.003 320 1	0.6	0.000 654 0	0.000 498 6	31.2
	75	0.002 659 8	0.002 624 5	1.3	0.000 424 9	0.000 381 4	11.4
	90	0.002 003 8	0.001 996 0	0.4	0.000 310 2	0.000 359 9	13.8
0.080	0	0.007 660 6	0.007 833 3	2.2	0.002 095 5	0.002 149 5	2.5
	15	0.007 393 3	0.007 658 3	3.5	0.001 998 8	0.002 001 9	0.2
	30	0.006 847 9	0.007 124 5	3.9	0.001 661 2	0.001 649 7	0.7
	45	0.006 133 0	0.006 286 6	2.4	0.001 316 2	0.001 239 5	6.2
	60	0.005 227 1	0.005 236 5	0.2	0.000 999 2	0.000 905 1	10.4
	75	0.004 170 4	0.004 153 6	0.4	0.000 768 5	0.000 720 9	6.6
	90	0.003 156 7	0.003 209 7	1.7	0.000 601 3	0.000 721 9	16.7

[a]ϕ characterizes the orientation of the field with $\phi = 0°$ corresponding to the field being parallel to the molecular axis. For CO, the field points from C to O at $\phi = 0°$.
[b]Computed with the aug-cc-pVTZ+3s3p3d3f/cc-pVTZ basis set and RI-MP2-aug-cc-pVTZ auxiliary basis set.
[c]Computed with the aug-cc-pVQZ+3s3p3d3f/cc-pVQZ basis set and RI-MP2-aug-cc-pVQZ auxiliary basis set.

real. The latter auxiliary bases represent our standard choice in this manuscript, whereas the former ones are similar to those we employed in our initial work on the subject.[62] We note that our implementation uses complex arithmetic for both basis sets; savings in computation time only stem from the different number of functions.

Figure 2 demonstrates the drastic savings that are made possible by the RI approximation. The canonical HF calculation for CO

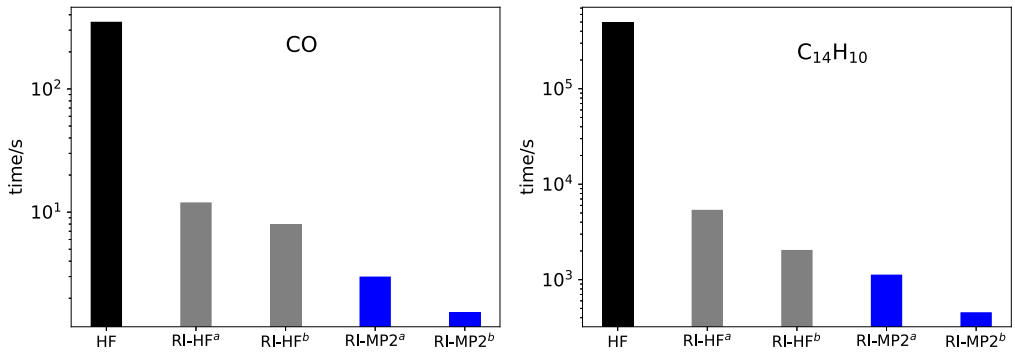

FIG. 2. Representative computation times of one complex energy for CO (left) and $C_{14}H_{10}$ (right) at different levels of theory computed on four cores of an Intel Xeon processor (3.2 GHz). The y-axis is in logarithmic scale. The basis set is of quadruple-ζ quality for CO and of triple-ζ quality for $C_{14}H_{10}$. Values denoted by "a" were computed with a partially complex-scaled auxiliary basis set, and values denoted by "b" were computed with an entirely real-valued auxiliary basis set. See main text and supplementary material for further details.

Published under license by AIP Publishing

takes around 6 min, whereas the RI-HF calculations take only 12 s or 8 s, respectively, depending on the auxiliary basis set. That is, the calculations are sped up by a factor of ~30–40.

For $C_{14}H_{10}$, it takes 139 h (almost 6 days) to compute one canonical HF energy. Because one always needs to carry out calculations for several values of the scaling angle (for the results reported in this article, we used 14 values) and because one is typically interested in Γ values at different strengths and orientations of the external field, an investigation of this system with canonical HF is not feasible. In contrast, an RI-HF calculation on $C_{14}H_{10}$ with the real-valued auxiliary basis set is done in less than 1 h and delivers essentially the same result. An investigation of the angular dependence of Γ as reported in Sec. IV can then be completed within one day for a molecule of this size.

The last two columns in both panels of Fig. 2 show the times required for the evaluation of the RI-MP2 correlation energy. For both molecules considered here, this part of the RI-MP2 calculation consumes less time than the HF part even though the formal scaling is higher. We note that this behavior is not special for complex-scaled calculations but, in fact, rather typical in Hermitian quantum chemistry as well and has been reported before repeatedly.[68] Significant additional speedups (by a factor of ~2.5 for $C_{14}H_{10}$) can again be realized by using real-valued auxiliary basis sets. As discussed in Sec. III A, the additional error is negligible.

For our present implementation, pentacene ($C_{22}H_{18}$) roughly represents the limit in terms of molecular size given that we used a maximum of 384 GB main memory for our calculations. Our modified aug-cc-pVTZ basis set comprises 2768 functions for pentacene, while the RI-MP2-aug-cc-pVTZ auxiliary basis set comprises 2976 functions. Using the corresponding modified aug-cc-pVQZ basis set, anthracene ($C_{14}H_{10}$) with 2732 basis functions and 3152 auxiliary functions represents the approximate limit. These restrictions stem from the fact that our implementation stores certain intermediates required for the evaluation of the RI-MP2 energy en bloc in memory; details are given in our previous publication.[62]

For pentacene and the modified aug-cc-pVTZ basis, the evaluation of the ionization rate at one particular field strength and orientation (that is, completion of 14 consecutive calculations using different values of the scaling angle θ) required 40–80 h on 8 cores of an Intel Xeon processor (3.2 GHz) depending on the convergence characteristics, which, in turn, depend on the field strength and orientation.

IV. EXEMPLARY APPLICATIONS: STATIC-FIELD IONIZATION OF POLYACENES

To demonstrate the usefulness of our implementation, we investigate in this section the ionization of polyacenes in static electric fields. Polyacenes[78–80] form an interesting class of molecules in this context for several reasons: Their electronic structure is highly anisotropic with the π-electrons being delocalized in only two directions. This is reflected in the dipole polarizability tensor, the component in the direction perpendicular to the molecular plane is much smaller than the other two.[81,82] One would, hence, expect highly anisotropic ionization rates, and our previous investigations of benzene and naphthalene[62] already illustrated that ionization of these molecules is hardest when the field is perpendicular to the molecular plane.

Furthermore, size effects can be studied in a straightforward manner for polyacenes because their electronic structure changes smoothly when aromatic rings are added. In addition, all acenes beyond naphthalene have structural isomers; the comparison of their ionization rates is insightful. Strong-field ionization of polyacenes is also interesting from the point of view of experiment as there are many setups where carbon-based molecules and materials interact with strong laser fields; for recent examples, see Refs. 83–85.

Besides our previous RI-MP2 investigation,[62] strong-field ionization of benzene has been studied using TD-DFT,[19,86] while that of naphthalene has been studied based on a semiclassical two-step model.[87] Theoretical investigations of larger acenes have not been reported to the best of our knowledge, but there are experimental data on the Coulomb explosion of naphthalene, anthracene, and tetracene that can be related to the ionization rates studied here.[88,89] We also note work on related molecules, for example, quantum dynamics simulations on the ionization of fullerene (C_{60}),[90] an experimental study on the ionization of estradiol ($C_{18}H_{24}O_2$),[91] and experimental and theoretical work on high-harmonic generation for heteroaromatics.[92,93]

A. Linearly fused acenes

Figure 3 shows ionization rates for five linearly fused polyacenes (benzene to pentacene) at field strengths of 0.04 a.u. and 0.06 a.u. All calculations were carried out with RI-MP2 and RI-HF using a modified aug-cc-pVTZ basis set. For benzene, naphthalene, and anthracene, we repeated these calculations with a corresponding aug-cc-pVQZ basis set; these results are available from the supplementary material. The deviations to Fig. 3 stay below 2%–3% at most orientations and for all three molecules; the maximum deviation is ~6%. This is in agreement with Table III given that all Γ values in Fig. 3 are between 10^{-3} a.u. and 10^{-1} a.u.

Figure 3 illustrates that the ionization rates grow monotonically with increasing molecular size. The same field strength of 0.04 a.u. leads to Γ values of $1–3 \times 10^{-3}$ a.u. for benzene but up to 8×10^{-2} a.u. for pentacene. This general trend can be easily related to the behavior of the ionization potentials; the lowest IP shrinks from 9.24 eV for benzene to 6.61 eV for pentacene. More interestingly, however, the anisotropy of Γ also changes. From benzene to pentacene, the ionization rate increases by less than a factor of 2 when the field is perpendicular to the molecular plane ($\phi = 90°$), but by more than a factor of 50 when the field is in the molecular plane ($\phi = 0°$). A similar trend is apparent in the dipole polarizability.[81,82] We also note that the orientation at which Γ is highest changes with system size; a pronounced maximum at 45° is obtained for benzene, whereas the ionization rate does not change much in the range from 0° to 45° for naphthalene and has its maximum at 0° for the larger acenes. The lowest Γ value is always obtained at 90° as is expected from the electronic structure of the acenes.

It can also be seen from Fig. 3 that the strength of the field makes an impact on the anisotropy of Γ. When going from $F = 0.04$ a.u. to 0.06 a.u., the ionization rate increases roughly by an order of magnitude for benzene and naphthalene, but more interestingly, the angular dependence changes. For benzene, the maximum in Γ moves from 45° to 60° and the global minimum moves from 90°

Published under license by AIP Publishing

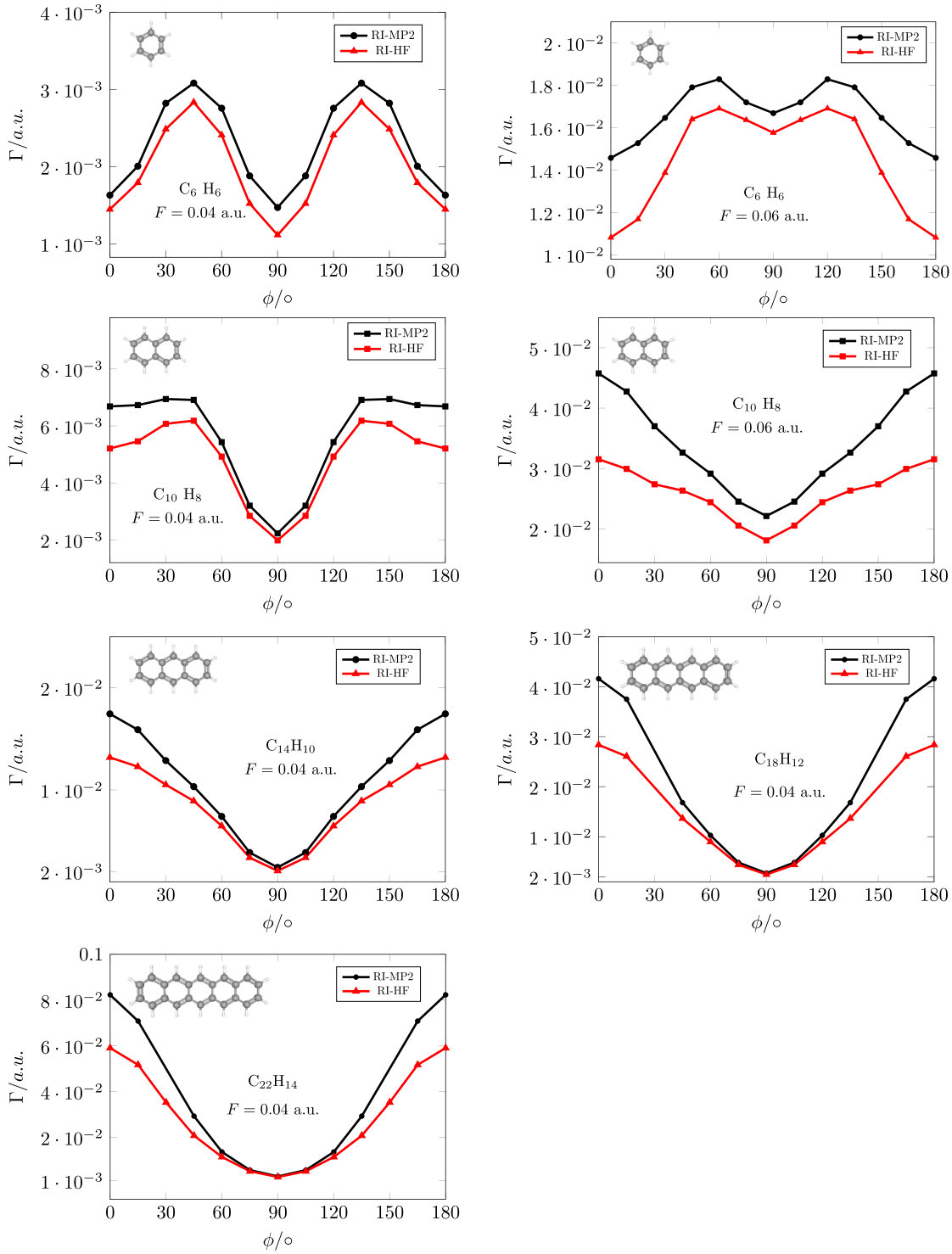

FIG. 3. Angle dependent ionization rates Γ of benzene (C_6H_6), naphthalene ($C_{10}H_8$), anthracene ($C_{14}H_{10}$), tetracene ($C_{18}H_{12}$), and pentacene ($C_{22}H_{14}$) at static field strengths of F = 0.04 a.u. and 0.06 a.u. computed at the RI-HF and RI-MP2 levels of theory using a modified aug-cc-pVTZ basis set and the standard RI-MP2-aug-cc-pVTZ auxiliary basis set. ϕ is the angle between the field and the mirror plane that cuts through all aromatic rings (for benzene: through an H atom) with ϕ = 90° corresponding to the field being perpendicular to the molecular plane. The two panels on the upper right have been published previously in Ref. 62 and use a slightly different auxiliary basis set.

Published under license by AIP Publishing

to 0°. We note that two independent TD-DFT studies with a time-dependent field of lower strength also found the minimum in Γ at 90° and the maximum at around 40°–45°.[19,86] For naphthalene, the plateau region between 0° and 45° disappears in favor of a clear maximum at 0°; that is, at the higher field strength, naphthalene behaves similarly to the larger acenes.

The comparison of RI-MP2 and RI-HF results in Fig. 3 illustrates the impact of electron correlation on the ionization rates. We found previously[60,62,71] and again in the present work (see Fig. 1) that HF substantially underestimates ionization rates in some cases, especially at low fields strengths. Figure 3 shows, however, that this trend is not uniform. Specifically, RI-MP2 and RI-HF results for benzene and naphthalene differ more at $F = 0.06$ a.u. than at 0.04 a.u. This difference also depends strongly on the orientation; RI-HF and RI-MP2 agree within 10%–20% at $\phi = 90°$ but can differ by more than 40% at $\phi = 0°$, in particular for the larger acenes. These differences are, however, still much smaller than what we observed previously for small molecules.[60]

B. Comparison of isomers: Anthracene and phenanthrene

Figure 4 compares RI-MP2 ionization rates for the two isomers anthracene and phenanthrene ($C_{14}H_{10}$) at different field strengths

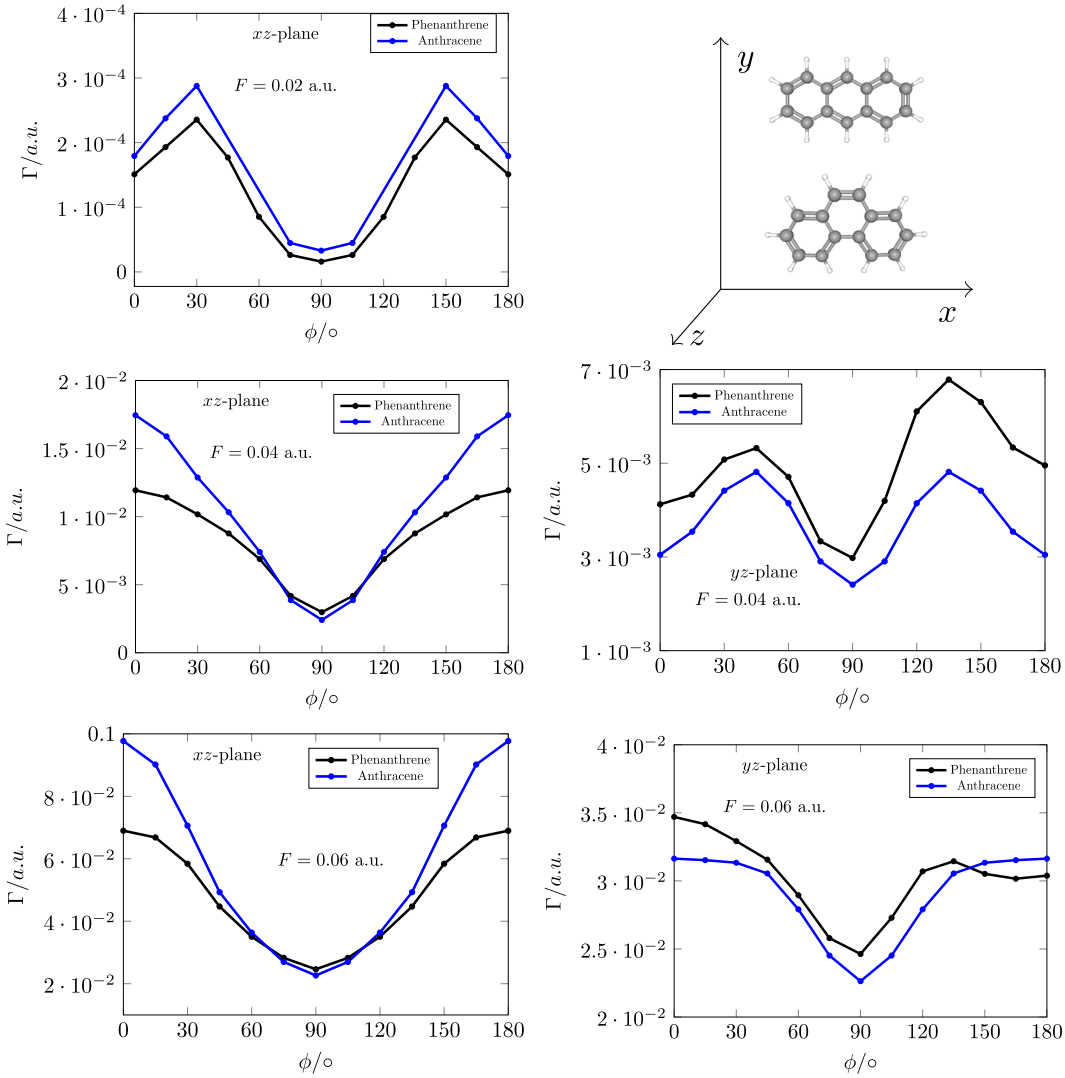

FIG. 4. Angle-dependent ionization rates Γ of the two isomers anthracene and phenanthrene ($C_{14}H_{10}$) at different field strengths and orientations computed with RI-MP2 using a modified aug-cc-pVTZ basis set and the standard RI-MP2-aug-cc-pVTZ auxiliary basis set. The field is in the *xz* plane or the *yz* plane, and ϕ is the angle between the field and the molecular plane (*xy*) with $\phi = 0°$ corresponding to the field being parallel to the molecular plane. The orientation of the molecules is also given in the top-right panel.

Published under license by AIP Publishing

and orientations. It is seen that Γ values of the two isomers are of the same order of magnitude at $F = 0.04$ a.u. and at $F = 0.06$ a.u. However, if the field is oriented along the x-axis, the ionization rate is always larger for anthracene, and this effect is especially pronounced at higher field strengths. If the field is oriented along the z-axis, that is, perpendicular to the molecular plane, Γ values for both molecules are much smaller overall but relatively higher for phenanthrene at the higher field strengths.

It is also apparent from Fig. 4 that the orientation at which the ionization rate assumes its maximum value changes with the field strength. At $F = 0.02$ a.u., ionization of both isomers is the easiest at $\phi = 30°$ in the xz-plane, but this peak moves to $\phi = 0°$ when the field strength is doubled. One can see that the increase in the field strength from 0.02 a.u. to 0.04 a.u. changes the ionization rate much more than a further increase from 0.04 a.u. to 0.06 a.u. We note that the basis set of triple-ζ quality used here is probably not fully adequate to evaluate the ionization rates at $F = 0.02$ a.u. with quantitative accuracy (see our discussion in Sec. III C); the overall trend in Γ is, however, very likely captured correctly.

Ionization rates in the yz-plane (right two panels of Fig. 4) reflect the lower symmetry of phenanthrene as compared to anthracene. It is seen that ionization rates are, in general, considerably lower for this orientation; this can be easily related to the lower spatial extent of the molecules along the y-axis as compared to the x-axis. The angular dependence of Γ again changes with the field strength; distinct peaks in Γ at $\phi = 45°$ are obtained with $F = 0.04$ a.u. but disappear when going to $F = 0.06$ a.u., which is somewhat similar to the behavior in the xz-plane and also to that of benzene and naphthalene shown in Fig. 3.

V. CONCLUSIONS AND OUTLOOK

We have investigated the performance of the RI-MP2 method for the computation of molecular static-field ionization rates. Our approach relies on the use of complex basis functions, which enables a description of the ionization process in terms of discrete Stark resonances with complex energies. The imaginary part of such a complex energy multiplied by a factor of two directly gives the ionization rate Γ.

As an exemplary application, we have studied the ionization of several polyacene molecules in static electric fields and the impact of molecular size and the field strength on the ionization rates. Although the overall behavior of Γ, in particular its large anisotropy, can be qualitatively explained by the electronic structure of the acenes, the quantitative modeling is more involved.

We found that the angular dependence of Γ changes in a nontrivial manner with the strength of the ionizing field. A possible reason could be that the relative importance of the different ionization channels changes. Notably, these anisotropies are not fully captured at the HF level of theory. Our results also confirm the previous finding[60,71] that smaller ionization rates demand larger basis sets because a larger region in space needs to be described for the tunneling process. A basis of triple-ζ quality becomes unreliable for Γ values below $\sim 10^{-3}$ a.u.

Our RI-MP2 method reproduces canonical MP2 and CCSD ionization rates within ~2% and 10%, respectively, but requires only a fraction of time. For a molecule of the size of anthracene ($C_{14}H_{10}$), the investigation of the angular dependence of Γ at a particular field strength can be completed within one day, and even for pentacene ($C_{22}H_{14}$), the same is possible within a few days.

An important convenient feature of the RI-MP2 method with complex basis functions is that the auxiliary basis set need not be larger than the original basis set, in contrast to recommendations for Hermitian RI-MP2 calculations. Furthermore, we have shown in this work theoretically and numerically that it is possible to use auxiliary basis sets that do not include any functions with complex-scaled exponent. The error in the ionization rate resulting from this truncation is typically less than 1% as compared to the more extended auxiliary basis sets from our previous work.[62]

Given the rather convincing performance of the present RI-MP2 method for the description of static-field ionization, we consider it worthwhile to extend our implementation to further quantities beyond the ionization rate[94,95] and to develop corresponding approaches for autoionizing states in larger molecules. For the latter type of the metastable state, the consistent description of the resonance together with its decay channels is key.[96] We believe that complex-variable approaches that combine the second-order approximate coupled-cluster method[97,98] with the RI approximation could be useful in this regard.

SUPPLEMENTARY MATERIAL

See the supplementary material for details about the basis sets and molecular structures, numerical results corresponding to Figs. 1–4, and additional results.

ACKNOWLEDGMENTS

We thank Travis H. Thompson (LMU Munich) for helpful discussions. This work has been supported by the Deutsche Forschungsgemeinschaft through Grant No. JA 2794/1-1 (Emmy Noether program) and by the Fonds der Chemischen Industrie.

DATA AVAILABILITY

The data that support the findings of this study are available within the article and in its supplementary material.

APPENDIX: PRODUCTS OF COMPLEX-SCALED GAUSSIAN FUNCTIONS

The basis sets used in CBF methods typically comprise two types of functions. The tighter basis functions are strictly real, whereas the exponents of the diffuse functions are complex scaled by a factor $e^{-2i\theta}$, $\theta \in \mathbb{R}$, according to Eq. (2). As a consequence, the following three types of products arise: between two real Gaussians, between two complex-scaled Gaussians, and between one real and one complex-scaled Gaussian. The latter two types shall be discussed in the following.

The product between two complex-scaled Gaussian functions centered at positions A and B takes the form

$$\chi_\mu \chi_\nu = N_\mu N_\nu S_\mu(r_A) S_\nu(r_B) \exp\left[-\alpha_\mu (\mathbf{r}-\mathbf{A})^2 e^{-2i\theta}\right] \times \exp\left[-\alpha_\nu (\mathbf{r}-\mathbf{B})^2 e^{-2i\theta}\right], \quad \text{(A1)}$$

Published under license by AIP Publishing

where all quantities are real before complex scaling is applied. Note that the normalization constants N_μ, N_ν are θ-dependent,[52] which is, however, not relevant to the point discussed here. Using the Gaussian product rule, Eq. (A1) can be rewritten as a single Gaussian function as

$$\chi_\mu\chi_\nu = N_\mu N_\nu S_\mu(r_A) S_\nu(r_B) \exp\left[\frac{-\alpha_\mu \alpha_\nu}{\alpha_\mu + \alpha_\nu} e^{-2i\theta} (\mathbf{A}-\mathbf{B})^2\right] \times \exp\left[-(\alpha_\mu + \alpha_\nu) e^{-2i\theta} (\mathbf{r}-\mathbf{C})^2\right], \tag{A2}$$

where the distant-dependent prefactor and the exponent of the product function are complex-scaled by the same angle as the individual functions. In addition, the product function is centered at the same location $\mathbf{C} \in \mathbb{R}^3$ as if the functions were not complex-scaled, that is,

$$\mathbf{C} = \frac{\alpha_\mu \mathbf{A} + \alpha_\nu \mathbf{B}}{\alpha_\mu + \alpha_\nu}. \tag{A3}$$

In contrast, the product between one real and one complex-scaled Gaussian cannot be written as a single Gaussian function centered at a real-valued location. This product takes the form

$$\chi_\mu\chi_\nu = N_\mu N_\nu S_\mu(r_A) S_\nu(r_B) \exp\left[-\alpha_\mu (\mathbf{r}-\mathbf{A})^2 e^{-2i\theta}\right] \times \exp\left[-\alpha_\nu (\mathbf{r}-\mathbf{B})^2\right]. \tag{A4}$$

Application of the product rule leads to

$$\chi_\mu\chi_\nu = N_\mu N_\nu S_\mu(r_A) S_\nu(r_B) \exp\left[\frac{-\alpha_\mu \alpha_\nu}{\alpha_\mu e^{-2i\theta} + \alpha_\nu} e^{-2i\theta} (\mathbf{A}-\mathbf{B})^2\right] \times \exp\left[-(\alpha_\mu e^{-2i\theta} + \alpha_\nu)(\mathbf{r}-\mathbf{C})^2\right]. \tag{A5}$$

This is a Gaussian function centered at

$$\mathbf{C} = \frac{\alpha_\mu e^{-2i\theta} \mathbf{A} + \alpha_\nu \mathbf{B}}{\alpha_\mu e^{-2i\theta} + \alpha_\nu}, \tag{A6}$$

that is, the location of the product function is not real-valued anymore.

Alternatively, it is possible to recast Eq. (A5) in terms of a Gaussian centered at a real-valued location multiplied by an additional oscillatory function. Starting from Eq. (A4), the exponential functions can be rewritten as

$$\exp\left[-\alpha_\mu(\mathbf{r}-\mathbf{A})^2 e^{-2i\theta}\right] \times \left[-\alpha_\nu(\mathbf{r}-\mathbf{B})^2\right] = \exp\left[i \sin(2\theta)\, \alpha_\mu (\mathbf{r}-\mathbf{A})^2\right] \exp\left[-\alpha_\mu(\mathbf{r}-\mathbf{A})^2 \cos(2\theta)\right] \times \exp\left[-\alpha_\nu(\mathbf{r}-\mathbf{B})^2\right]. \tag{A7}$$

Applying the Gaussian product rule to the last two real-valued factors, we obtain

$$\chi_\mu\chi_\nu = N_\mu N_\nu S_\mu(r_A) S_\nu(r_B) \exp\left[i \sin(2\theta)\, \alpha_\mu (\mathbf{r}-\mathbf{A})^2\right] \times \exp\left[\frac{-\cos(2\theta)\, \alpha_\mu \alpha_\nu}{\alpha_\mu \cos(2\theta) + \alpha_\nu} (\mathbf{A}-\mathbf{B})^2\right] \times \exp\left[-(\alpha_\mu \cos(2\theta) + \alpha_\nu)(\mathbf{r}-\mathbf{C})^2\right], \tag{A8}$$

where $\mathbf{C}$ is now real-valued,

$$\mathbf{C} = \frac{\alpha_\mu \cos(2\theta)\, \mathbf{A} + \alpha_\nu \mathbf{B}}{\alpha_\mu \cos(2\theta) + \alpha_\nu}, \tag{A9}$$

but the overall expression is not just a simple Gaussian function.

REFERENCES

[1] N. Moiseyev, *Non-Hermitian Quantum Mechanics*, 1st ed. (Cambridge University Press, 2011).
[2] T.-C. Jagau, K. B. Bravaya, and A. I. Krylov, "Extending quantum chemistry of bound states to electronic resonances," Annu. Rev. Phys. Chem. **68**, 525–553 (2017).
[3] N. Moiseyev and M. Lein, "Non-Hermitian quantum mechanics for high-order harmonic generation spectra," J. Phys. Chem. A **107**, 7181–7188 (2003).
[4] C. Winterfeldt, C. Spielmann, and G. Gerber, "Optimal control of high-harmonic generation," Rev. Mod. Phys. **80**, 117–140 (2008).
[5] K. L. Ishikawa, "High-harmonic generation," in *Advances in Solid-State Lasers* (In Tech, 2010), pp. 439–464.
[6] N. Suárez, A. Chacón, M. F. Ciappina, J. Biegert, and M. Lewenstein, "Above-threshold ionization and photoelectron spectra in atomic systems driven by strong laser fields," Phys. Rev. A **92**, 063421 (2015).
[7] N. Suárez, A. Chacón, M. F. Ciappina, B. Wolter, J. Biegert, and M. Lewenstein, "Above-threshold ionization and laser-induced electron diffraction in diatomic molecules," Phys. Rev. A **94**, 043423 (2016).
[8] M. Spanner, O. Smirnova, P. B. Corkum, and M. Y. Ivanov, "Reading diffraction images in strong field ionization of diatomic molecules," J. Phys. B: At., Mol. Opt. Phys. **37**, L243–L250 (2004).
[9] M. Meckel, D. Comtois, D. Zeidler, A. Staudte, D. Pavicic, H. C. Bandulet, H. Pepin, J. C. Kieffer, R. Dorner, D. M. Villeneuve, and P. B. Corkum, "Laser-induced electron tunneling and diffraction," Science **320**, 1478–1482 (2008).
[10] C. I. Blaga, J. Xu, A. D. DiChiara, E. Sistrunk, K. Zhang, P. Agostini, T. A. Miller, L. F. DiMauro, and C. D. Lin, "Imaging ultrafast molecular dynamics with laser-induced electron diffraction," Nature **483**, 194–197 (2012).
[11] J. S. Parker, B. J. S. Doherty, K. T. Taylor, K. D. Schultz, C. I. Blaga, and L. F. DiMauro, "High-energy cutoff in the spectrum of strong-field nonsequential double ionization," Phys. Rev. Lett. **96**, 133001 (2006).
[12] J. S. Parker, G. S. J. Armstrong, M. Boca, and K. T. Taylor, "From the UV to the static-field limit: Rates and scaling laws of intense-field ionization of helium," J. Phys. B: At., Mol. Opt. Phys. **42**, 134011 (2009).
[13] M. A. Lysaght, L. R. Moore, L. A. A. Nikolopoulos, J. S. Parker, H. W. van der Hart, and K. T. Taylor, "*Ab initio* methods for few- and many-electron atomic systems in intense short-pulse laser light," in *Quantum Dynamic Imaging* (Springer, New York, 2011), pp. 107–134.
[14] P. Krause, J. A. Sonk, and H. B. Schlegel, "Strong field ionization rates simulated with time-dependent configuration interaction and an absorbing potential," J. Chem. Phys. **140**, 174113 (2014).
[15] P. Krause and H. B. Schlegel, "Angle-dependent ionization of small molecules by time-dependent configuration interaction and an absorbing potential," J. Phys. Chem. Lett. **6**, 2140–2146 (2015).
[16] P. Hoerner, M. K. Lee, and H. B. Schlegel, "Angular dependence of strong field ionization of N_2 by time-dependent configuration interaction using density functional theory and the Tamm-Dancoff approximation," J. Chem. Phys. **151**, 054102 (2019).
[17] S. Pabst, A. Sytcheva, O. Geffert, and R. Santra, "Stability of the time-dependent configuration-interaction-singles method in the attosecond and strong-field regimes: A study of basis sets and absorption methods," Phys. Rev. A **94**, 033421 (2016).
[18] A. Sissay, P. Abanador, F. Mauger, M. Gaarde, K. J. Schafer, and K. Lopata, "Angle-dependent strong-field molecular ionization rates with tuned range-separated time-dependent density functional theory," J. Chem. Phys. **145**, 094105 (2016).
[19] E. Yahel and A. Natan, "Effect of multiorbital contributions to strong-field ionization of benzene derivatives," Phys. Rev. A **98**, 053421 (2018).
[20] P. Sándor, A. Sissay, F. Mauger, M. W. Gordon, T. T. Gorman, T. D. Scarborough, M. B. Gaarde, K. Lopata, K. J. Schafer, and R. R. Jones, "Angle-dependent strong-field ionization of halomethanes," J. Chem. Phys. **151**, 194308 (2019).
[21] F. Zapata, E. Luppi, and J. Toulouse, "Linear-response range-separated density-functional theory for atomic photoexcitation and photoionization spectra," J. Chem. Phys. **150**, 234104 (2019).

Published under license by AIP Publishing

[22]R. Kosloff and D. Kosloff, "Absorbing boundaries for wave propagation problems," J. Comput. Phys. **63**, 363–376 (1986).
[23]U. V. Riss and H.-D. Meyer, "Calculation of resonance energies and widths using the complex absorbing potential method," J. Phys. B: At., Mol. Opt. Phys. **26**, 4503–4536 (1993).
[24]U. V. Riss and H. D. Meyer, "Investigation on the reflection and transmission properties of complex absorbing potentials," J. Chem. Phys. **105**, 1409–1419 (1996).
[25]L. Greenman, P. J. Ho, S. Pabst, E. Kamarchik, D. A. Mazziotti, and R. Santra, Phys. Rev. A **82**, 023406 (2010).
[26]E. Balslev and J. M. Combes, "Spectral properties of many-body Schrödinger operators with dilatation-analytic interactions," Commun. Math. Phys. **22**, 280–294 (1971).
[27]J. Aguilar and J. M. Combes, "A class of analytic perturbations for one-body Schrödinger Hamiltonians," Commun. Math. Phys. **22**, 269–279 (1971).
[28]C. W. McCurdy, C. K. Stroud, and M. K. Wisinski, "Solving the time-dependent Schrödinger equation using complex-coordinate contours," Phys. Rev. A **43**, 5980–5990 (1991).
[29]A. Scrinzi and N. Elander, "A finite element implementation of exterior complex scaling for the accurate determination of resonance energies," J. Chem. Phys. **98**, 3866–3875 (1993).
[30]A. Scrinzi, "Infinite-range exterior complex scaling as a perfect absorber in time-dependent problems," Phys. Rev. A **81**, 053845 (2010).
[31]Y. Orimo, T. Sato, A. Scrinzi, and K. L. Ishikawa, "Implementation of the infinite-range exterior complex scaling to the time-dependent complete-active-space self-consistent-field method," Phys. Rev. A **97**, 023423 (2018).
[32]A. Scrinzi, M. Y. Ivanov, R. Kienberger, and D. M. Villeneuve, "Attosecond physics," J. Phys. B: At., Mol. Opt. Phys. **39**, R1–R37 (2006).
[33]M. V. Ammosov, N. B. Delone, and V. P. Krainov, "Tunnel ionization of complex atoms and of atomic ions in an alternating electromagnetic field," Sov. Phys. JETP **64**, 1191–1194 (1986).
[34]X. M. Tong, Z. X. Zhao, and C. D. Lin, "Theory of molecular tunneling ionization," Phys. Rev. A **66**, 033402 (2002).
[35]X. M. Tong and C. D. Lin, "Empirical formula for static field ionization rates of atoms and molecules by lasers in the barrier-suppression regime," J. Phys. B: At., Mol. Opt. Phys. **38**, 2593–2600 (2005).
[36]O. I. Tolstikhin, L. B. Madsen, and T. Morishita, "Weak-field asymptotic theory of tunneling ionization in many-electron atomic and molecular systems," Phys. Rev. A **89**, 013421 (2014).
[37]L. B. Madsen, F. Jensen, A. I. Dnestryan, and O. I. Tolstikhin, "Structure factors for tunneling ionization rates of molecules: General Hartree-Fock-based integral representation," Phys. Rev. A **96**, 013423 (2017).
[38]L. Yue, S. Bauch, and L. B. Madsen, "Electron correlation in tunneling ionization of diatomic molecules: An application of the many-electron weak-field asymptotic theory with a generalized-active-space partition scheme," Phys. Rev. A **96**, 043408 (2017).
[39]P. K. Samygin, T. Morishita, and O. I. Tolstikhin, "Weak-field asymptotic theory of tunneling ionization from nearly degenerate states," Phys. Rev. A **98**, 033401 (2018).
[40]V. P. Majety, A. Zielinski, and A. Scrinzi, "Photoionization of few electron systems: A hybrid coupled channels approach," New J. Phys. **17**, 063002 (2015).
[41]V. P. Majety and A. Scrinzi, "Static field ionization rates for multi-electron atoms and small molecules," J. Phys. B: At., Mol. Opt. Phys. **48**, 245603 (2015).
[42]I. I. Fabrikant and L. B. Zhao, "Green-function approach to the theory of tunneling ionization," Phys. Rev. A **91**, 053412 (2015).
[43]M. Z. Milošević and N. S. Simonović, "Calculations of rates for strong-field ionization of alkali-metal atoms in the quasistatic regime," Phys. Rev. A **91**, 023424 (2015).
[44]W. P. Reinhardt, "Method of complex coordinates: Application to the Stark effect in hydrogen," Int. J. Quantum Chem. **10**, 359–367 (1976).
[45]I. W. Herbst and B. Simon, "Stark effect revisited," Phys. Rev. Lett. **41**, 67–69 (1978).
[46]I. W. Herbst, "Dilation analyticity in constant electric field. I. The two body problem," Commun. Math. Phys. **64**, 279–298 (1979).
[47]I. W. Herbst and B. Simon, "Dilation analyticity in constant electric field. II. N-body problem, Borel summability," Commun. Math. Phys. **80**, 181 (1981).
[48]C. A. Nicolaides and S. I. Themelis, "Theory of the resonances of the LoSurdo-Stark effect," Phys. Rev. A **45**, 349–357 (1992).
[49]B. Simon, "The definition of molecular resonance curves by the method of exterior complex scaling," Phys. Lett. A **71**, 211–214 (1979).
[50]C. W. McCurdy and T. N. Rescigno, "Extension of the method of complex basis functions to molecular resonances," Phys. Rev. Lett. **41**, 1364–1368 (1978).
[51]N. Moiseyev and C. Corcoran, "Autoionizing states of H_2 and H_2^- using the complex-scaling method," Phys. Rev. A **20**, 814–817 (1979).
[52]A. F. White, M. Head-Gordon, and C. W. McCurdy, "Complex basis functions revisited: Implementation with applications to carbon tetrafluoride and aromatic N-containing heterocycles within the static-exchange approximation," J. Chem. Phys. **142**, 054103 (2015).
[53]T. N. Rescigno, A. E. Orel, and C. W. McCurdy, "Application of complex coordinate SCF techniques to a molecular shape resonance: The $^2\Pi_g$ state of N_2^-," J. Chem. Phys. **73**, 6347–6348 (1980).
[54]C. W. McCurdy, T. N. Rescigno, E. R. Davidson, and J. G. Lauderdale, "Applicability of self-consistent field techniques based on the complex coordinate method to metastable electronic states," J. Chem. Phys. **73**, 3268–3273 (1980).
[55]A. F. White, C. W. McCurdy, and M. Head-Gordon, "Restricted and unrestricted non-Hermitian Hartree-Fock: Theory, practical considerations, and applications to metastable molecular anions," J. Chem. Phys. **143**, 074103 (2015).
[56]S. Yabushita and C. W. McCurdy, "Feshbach resonances in electron–molecule scattering by the complex multiconfiguration SCF and configuration interaction procedures: The $^1\Sigma_g^+$ autoionizing states of H_2," J. Chem. Phys. **83**, 3547–3559 (1985).
[57]M. Honigmann, R. J. Buenker, and H.-P. Liebermann, "Complex self-consistent field and multireference single- and double-excitation configuration interaction calculations for the $^2\Pi_g$ resonance state of N_2^-," J. Chem. Phys. **125**, 234304 (2006).
[58]M. Honigmann, R. J. Buenker, and H.-P. Liebermann, "Complex multireference configuration interaction calculations employing a coupled diabatic representation for the $^2\Pi_g$ resonance states of N_2^-," J. Chem. Phys. **131**, 034303 (2009).
[59]A. F. White, E. Epifanovsky, C. W. McCurdy, and M. Head-Gordon, "Second order Møller-Plesset and coupled cluster singles and doubles methods with complex basis functions for resonances in electron-molecule scattering," J. Chem. Phys. **146**, 234107 (2017).
[60]T.-C. Jagau, "Coupled-cluster treatment of molecular strong-field ionization," J. Chem. Phys. **148**, 204102 (2018).
[61]T. H. Thompson, C. Ochsenfeld, and T.-C. Jagau, "A Schwarz inequality for complex basis function methods in non-Hermitian quantum chemistry," J. Chem. Phys. **151**, 184104 (2019).
[62]M. Hernández Vera and T.-C. Jagau, "Resolution-of-the-identity approximation for complex-scaled basis functions," J. Chem. Phys. **151**, 111101 (2019).
[63]E. J. Baerends, D. E. Ellis, and P. Ros, "Self-consistent molecular Hartree-Fock-Slater calculations. I. The computational procedure," Chem. Phys. **2**, 41–51 (1973).
[64]J. L. Whitten, "Coulombic potential energy integrals and approximations," J. Chem. Phys. **58**, 4496–4501 (1973).
[65]B. I. Dunlap, J. W. D. Connolly, and J. R. Sabin, "On some approximations in applications of $X\alpha$ theory," J. Chem. Phys. **71**, 3396–3402 (1979).
[66]O. Vahtras, J. Almlöf, and M. W. Feyereisen, "Integral approximations for LCAO-SCF calculations," Chem. Phys. Lett. **213**, 514–518 (1993).
[67]M. Feyereisen, G. Fitzgerald, and A. Komornicki, "Use of approximate integrals in *ab initio* theory. An application in MP2 energy calculations," Chem. Phys. Lett. **208**, 359–363 (1993).
[68]F. Weigend, "A fully direct RI-HF algorithm: Implementation, optimised auxiliary basis sets, demonstration of accuracy and efficiency," Phys. Chem. Chem. Phys. **4**, 4285–4291 (2002).
[69]F. Weigend, M. Kattannek, and R. Ahlrichs, "Approximated electron repulsion integrals: Cholesky decomposition versus resolution of the identity methods," J. Chem. Phys. **130**, 164106 (2009).

Published under license by AIP Publishing

[70]Y. Shao, Z. Gan, E. Epifanovsky, A. T. Gilbert, M. Wormit *et al.*, "Advances in molecular quantum chemistry contained in the Q-Chem 4 program package," Mol. Phys. **113**, 184–215 (2015).
[71]T.-C. Jagau, "Investigating tunnel and above-barrier ionization using complex-scaled coupled-cluster theory," J. Chem. Phys. **145**, 204115 (2016).
[72]F. Weigend, A. Köhn, and C. Hättig, "Efficient use of the correlation consistent basis sets in resolution of the identity MP2 calculations," J. Chem. Phys. **116**, 3175–3183 (2002).
[73]Here and in the following, we use parentheses for Mulliken notation and chevrons for Dirac notation. In non-Hermitian quantum mechanics, it is also common to indicate the c-product by using parentheses. In this article, the c-product is used throughout, but we do not indicate this by using a special notation.
[74]N. Moiseyev, P. R. Certain, and F. Weinhold, "Resonance properties of complex-rotated Hamiltonians," Mol. Phys. **36**, 1613–1630 (1978).
[75]F. Weigend, M. Häser, H. Patzelt, and R. Ahlrichs, "RI-MP2: Optimized auxiliary basis sets and demonstration of efficiency," Chem. Phys. Lett. **294**, 143–152 (1998).
[76]W. Skomorowski and A. I. Krylov, "Real and imaginary excitons: Making sense of resonance wave functions by using reduced state and transition density matrices," J. Phys. Chem. Lett. **9**, 4101–4108 (2018).
[77]H. A. Früchtl, R. A. Kendall, R. J. Harrison, and K. G. Dyall, "An implementation of RI-SCF on parallel computers," Int. J. Quantum Chem. **64**, 63–69 (1997).
[78]J. E. Anthony, "The larger acenes: Versatile organic semiconductors," Angew. Chem., Int. Ed. **47**, 452–483 (2007).
[79]Z. Sun, Q. Ye, C. Chi, and J. Wu, "Low band gap polycyclic hydrocarbons: From closed-shell near infrared dyes and semiconductors to open-shell radicals," Chem. Soc. Rev. **41**, 7857–7889 (2012).
[80]S. Dong, A. Ong, and C. Chi, "Photochemistry of various acene based molecules," J. Photochem. Photobiol., C **38**, 27–46 (2019).
[81]J. R. Hammond, K. Kowalski, and W. A. deJong, "Dynamic polarizabilities of polyaromatic hydrocarbons using coupled-cluster linear response theory," J. Chem. Phys. **127**, 144105 (2007).
[82]M. Huzak and M. S. Deleuze, "Benchmark theoretical study of the electric polarizabilities of naphthalene, anthracene, and tetracene," J. Chem. Phys. **138**, 024319 (2013).
[83]A. Kucher, L. M. Jackson, J. O. Lerach, A. N. Bloom, N. J. Popczun, A. Wucher, and N. Winograd, "Near infrared (NIR) strong field ionization and imaging of C_{60} sputtered molecules: Overcoming matrix effects and improving sensitivity," Anal. Chem. **86**, 8613–8620 (2014).
[84]I. Crassee, L. Gallmann, G. Gäumann, M. Matthews, H. Yanagisawa, T. Feurer, M. Hengsberger, U. Keller, J. Osterwalder, H. J. Wörner, and J. P. Wolf, "Strong field transient manipulation of electronic states and bands," Struct. Dyn. **4**, 061505 (2017).
[85]T. Higuchi, C. Heide, K. Ullmann, H. B. Weber, and P. Hommelhoff, "Light-field-driven currents in graphene," Nature **550**, 224–228 (2017).
[86]T. Otobe and K. Yabana, "Density-functional calculation for the tunnel ionization rate of hydrocarbon molecules," Phys. Rev. A **75**, 062507 (2007).
[87]D. Dimitrovski, J. Maurer, H. Stapelfeldt, and L. B. Madsen, "Strong-field ionization of three-dimensionally aligned naphthalene molecules: Orbital modification and imprints of orbital nodal planes," J. Phys. B: At., Mol. Opt. Phys. **48**, 245601 (2015).
[88]A. N. Markevitch, N. P. Moore, and R. J. Levis, "The influence of molecular structure on strong field energy coupling and partitioning," Chem. Phys. **267**, 131 (2001).
[89]A. N. Markevitch, D. A. Romanov, S. M. Smith, and R. J. Levis, "Probing strong-field electron-nuclear dynamics of polyatomic molecules using proton motion," Phys. Rev. A **75**, 053402 (2007).
[90]Z.-Z. Lin and X. Chen, "Ultrafast dynamics and fragmentation of C_{60} in intense laser pulses," Phys. Lett. A **377**, 797–800 (2013).
[91]A. Kucher, A. Wucher, and N. Winograd, "Strong field ionization of β-estradiol in the IR: Strategies to optimize molecular postionization in secondary neutral mass spectrometry," J. Phys. Chem. C **118**, 25534–25544 (2014).
[92]A. F. Alharbi, A. E. Boguslavskiy, N. Thiré, B. E. Schmidt, F. Légaré, T. Brabec, M. Spanner, and V. R. Bhardwaj, "Sensitivity of high-order-harmonic generation to aromaticity," Phys. Rev. A **92**, 041801 (2015).
[93]A. F. Alharbi, A. E. Boguslavskiy, N. Thiré, G. S. Thekkadath, S. Patchkovskii, B. E. Schmidt, F. Légaré, T. Brabec, V. R. Bhardwaj, and M. Spanner, "Effects of nodal planes on strong-field ionization and high-order-harmonic generation in ring-type molecules," Phys. Rev. A **96**, 043402 (2017).
[94]T.-C. Jagau and A. I. Krylov, "Characterizing metastable states beyond energies and lifetimes: Dyson orbitals and transition dipole moments," J. Chem. Phys. **144**, 054113 (2016).
[95]Z. Benda and T.-C. Jagau, "Analytic gradients for the complex absorbing potential equation-of-motion coupled-cluster method," J. Chem. Phys. **146**, 031101 (2017).
[96]T.-C. Jagau and A. I. Krylov, "Complex absorbing potential equation-of-motion coupled-cluster method yields smooth and internally consistent potential energy surfaces and lifetimes for molecular resonances," J. Phys. Chem. Lett. **5**, 3078–3085 (2014).
[97]O. Christiansen, H. Koch, and P. Jørgensen, "The second-order approximate coupled-cluster singles and doubles model CC2," Chem. Phys. Lett. **243**, 409–418 (1995).
[98]C. Hättig and F. Weigend, "CC2 excitation energy calculations on large molecules using the resolution of the identity approximation," J. Chem. Phys. **113**, 5154–5161 (2000).

Published under license by AIP Publishing